Application of Artificial Neural Networks in Modeling Limestone–SO_2 Reaction

Jayanta K. Bandyopadhyay, Senthil Annamalai, and K. Lal Gauri
Geosciences, University of Louisville, Louisville, KY 40292

Four varieties of limestone distinguished on the basis of pore-size distributions were exposed in dynamic 10-, 20- and 50-ppm SO_2 atmospheres for up to 500 h at 25°C and 100% rh. The resulting conversion of the limestone was measured as a function of the reaction product formed and the change in porosity. These conversions could be predicted correctly using either the shrinking unreacted core model or the distributed pore model. An artificial neural network (ANN) was also trained for the purpose. All three approaches predicted conversions that fitted well with the observed data; however, those predicted by ANN were the most accurate. Further, the weights determined for ANN on the basis of three limestone varieties also accurately predicted the conversions of the fourth variety for which no information was supplied in the training phase, showing that ANN can also be used successfully to estimate gas–solid noncatalytic reactions.

Introduction

This article has grown from our research on the weathering of carbonate rocks in the modern SO_2-enriched atmospheres of industrial countries. Our previous studies included dolomite and marble as the reactant species (Tambe et al., 1994; Yerrapragada et al., 1992, 1994). Here we report the results of our work upon four varieties of U.S. limestone commonly used in architecture. These limestones consist essentially of the mineral calcite, $CaCO_3$.

The varieties of limestone used in this study are the Bedford Limestone (BD) from Indiana, and the Cordova Shell (CS), Cordova Cream (CR), and Louder Limestone (LD) from Texas. The Bedford Limestone is of Mississippian age, while the varieties from Texas are much younger, being of Cretaceous age. Due to the age difference and the difference in their depositional environment and diagenetic processes (Chowdhury et al., 1990), these varieties of limestone possess distinct porosity and pore-size distributions. Thus, the magnitude of their reactivity also varies. The large spectrum of pore-size distributions possessed by the limestones studied make the results of this work applicable to other varieties of porous carbonate rocks.

Correspondence concerning this article should be addressed to K. L. Gauri.
J. K. Bandyopadhyay is from the Division of Chemical Engineering of the National Chemical Laboratory, Poona, India, appointed as a Postdoctoral Research Associate in Geosciences.
S. Annamalai is a graduate student in the Chemical Engineering Department.

Related work by others is on calcined limestone, CaO, which has a very high porosity, and in which the reactions were carried out at thousands of ppm of SO_2 concentrations at a highly elevated temperature in a nearly dry condition (Bhatia and Perlmutter, 1980; Hartman and Coughlin, 1976). These and other studies, such as Snow et al. (1988), and Zarkanitis and Sotirchos (1989), have modeled the reactions on the concepts of pore and grain-theory models. In this study we present results based upon such models, but our emphasis is upon the application of the computational system artificial neural networks (ANNs). We show that ANNs predicted the magnitude of said reactions better than the other approaches.

Experimental Methods and Materials

The sample brickets, approximately 2.5 cm × 1.7 cm × 0.5 cm, were cut from the limestone types given in the Introduction. After being polished with 400 grit silicon carbide powder to ensure uniform surfaces, the samples were cleaned ultrasonically in deionized water to remove any abrasive and dried at 105°C. Samples were also repeatedly washed in deionized water to remove any soluble salts present in the stone. Clean samples were thus produced as verified by the ion chromatography analysis.

Some of the clean samples were thoroughly ground in an agate pestle and were analyzed for mineralogical composition

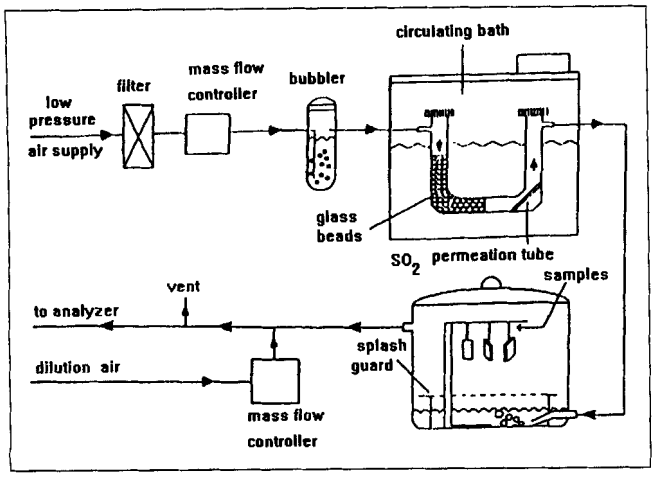

Figure 1. Reaction chamber.

by X-ray diffraction spectroscopy using Cu K-alpha radiation at 40 kV and 45 mA for 2θ values in the range of 3° to 75°. These data were quantitatively analyzed by the Rietwald technique where the observed pattern for each phase was compared with the calculated single-crystal structural data.

Samples were also digested in HCl and analyzed quantitatively by atomic absorption spectroscopy (AA) for Ca^{2+} and Mg^{2+}, the common cations expected to occur in limestone. Other samples were exposed in a reactor.

The reaction chamber, a modified 10-L desiccator, is shown in Figure 1. The experimental design, described in detail in Yerrapragada et al. (1994), is concisely given below.

The reaction was carried out in a 25°C constant-temperature room and the relative humidity in the chamber was maintained at nearly 100%, but it was ensured that moisture condensation did not occur upon stone surfaces by routing the airstream through or outside the bubbler. Atmospheres containing 10, 20, and 50 ppm SO_2 were generated by passing compressed air over permeation tubes (VICI Metronics). The concentration of SO_2 in the chamber was determined from permeation rates obtained from the weight loss of permeation tubes and confirmed by the measurement of the gas at the exit of the chamber using a Columbia Scientific Industries (CSI) analyzer. The compressed-air flow rate of nearly 800 cc/min over tubes of permeation rates of 2.09×10^4, 4.19×10^4, and 10.5×10^4 ng/min produced a concentration of SO_2 of 10, 20, and 50 ppm, respectively.

The reaction product consisted of gypsum ($CaSO_4\cdot2H_2O$), as determined by X-ray diffraction. For the quantitative analysis, however, gypsum, a water-soluble salt (solubility in pure water at 25°C is 14 mg/L, measured; Weast, 1974), was leached into a measured volume of deionized water immediately after the specimens were removed from the reaction chamber. Sometimes it was necessary to wash the samples repeatedly for varying periods of time to leach the entire reaction product.

The leachate was analyzed quantatively by ion chromatography using DIONEX-100 for the SO_4^{2-} and atomic absorption spectroscopy for Ca^{2+} ions. SO_4^{2-} was converted to gypsum, which was then related to the loss of $CaCO_3$ by mass balance. The conversion, shown in the illustrations of this article, is the ratio of the converted to the initial mass of limestone (mg/g).

Mercury intrusion porosimetry (MIP) was used to determine porosity, pore-size distributions, pore-surface area and the bulk density of unreacted samples, as well as those of the reacted samples after the reaction product had been leached. Porosity was also measured by a water-absorption technique in which the sample was immersed in water for 24 h after being evacuated at 660-torr mercury pressure in a vacuum chamber.

MIP is a destructive technique, that is, samples injected with mercury cannot be used again for other purposes. Therefore, our measurement of the change in porosity, used in the pore model, was based upon porosities obtained by the water absorption technique only.

Brickets, similar to those used in the reaction chamber, were used in Micromeritics Pore Sizer 9320 to obtain data for mercury intrusion, extrusion, and reintrusion in the pressure range of 3–30,000 psia (21–207,000 kPa). The low-pressure runs were made between 3 and 14 psia and the high-pressure runs between 15 and 30,000 psia (103 and 207,000 kPa). The pore sizer collected and processed the data automatically for selected pressure points. The pore volume of pressure points between the experimental points was generated by the spline interpolation algorithm. The pore size was calculated from the applied pressure, P(psia), as $180/P$, using the classic Washburn (1921) equation:

$$d = \frac{-4\gamma\,|\cos\theta\,|}{P}, \tag{1}$$

where $d(\mu m)$ is the diameter of the pore intruded at the applied pressure, P(psia), γ, and θ are the surface tension (485 dyne/cm), and the contact angle (130°) of mercury with the pore wall.

Mathematical Modeling

The reaction of limestone with SO_2 can be evaluated using the shrinking unreacted core model for product conversion (Szekely et al., 1976; Doraiswamy and Sharma, 1984; Cao et al., 1995) and the distributed pore model (Zarkanitis and Sotirchos, 1989) for change in porosity. We will apply these models as well as ANN to evaluate these reactions. These three models are briefly described below.

Shrinking unreacted-core model

We have successfully applied the shrinking unreacted-core model to predict the reaction of dolomite [$CaMg(CO_3)_2$] in SO_2 atmospheres (Tambe et al., 1991). The reaction kinetics and diffusion are the controlling parameters in these reactions. The final expression for conversion (x) can be given by

$$\frac{dx}{dt} = \frac{3K_s}{\dfrac{1}{(1-x)^{2/3}} + \gamma\left(\dfrac{1}{(1-x)^{1/3}} - \dfrac{1}{(1+Px)^{1/3}}\right)} \tag{2}$$

$$K_s = \frac{k_s C_s}{R_0 N_0} \tag{3a}$$

$$\gamma = \frac{R_o k_s}{D_e} \tag{3b}$$

$$P = N_0(V_p - V_r), \tag{3c}$$

where N_0 represents the initial concentration of the solid reactant; k_s the kinetic constant of the surface reaction; C_s the surface concentration of the gas; R_0 the equivalent initial radius of the grain; V_p and V_r the molar volume of solid product and reactant; D_e the diffusivity of Ca^{2+} ions. The surface gas concentration (C_s), was calculated by the relationship given by Tambe et al. (1994).

Distributed-pore model

The term "distributed pore model" is adapted from Zarkanitis and Sotirchos (1989). This model is one of various percolation theory models (Mohanty et al., 1994; Yortsos and Sharma, 1986; Fuertes and Marban, 1994) that relate chemical conversion of the reactant to the change in its porosity.

The pore network in a porous medium can be described by the pore-size distribution and the coordination number (Z) defined as the number of pores emanating from a site or number of pores accessible in the network. According to Fisher and Essam (1961) the accessible porosity of a Z coordinated network can be written as

$$\phi^A = \phi\left(1 - [\phi^R/\phi]^{(2Z-2)/(Z-2)}\right), \tag{4a}$$

where, ϕ and ϕ^A are the total and the accessible porosity, and ϕ^R can be obtained from the following relationship:

$$\phi^R(1-\phi^R)^{(Z-2)} - \phi(1-\phi)^{(Z-2)} = 0. \tag{4b}$$

Equation 4b is valid when $\phi > \phi_c$, where

$$\phi_c = \frac{1}{(Z-1)}. \tag{4c}$$

According to Reyes and Jensen (1986) the relation of accessible internal surface area, a^A, to the pore structure can be evaluated by

$$a^A = K(\phi[1-\phi] - \phi^I[1-\phi^I]), \tag{5}$$

where K, a form of connectivity coefficient, is obtained by matching initial surface area to the accessible surface area and where, ϕ^I is the isolated porosity, obtained from the difference between the total porosity, ϕ, and the accessible porosity, ϕ^A. Although we were unable to obtain a value of K on the basis of surface area that could express the conversion data obtained in our experiments, nonetheless the value of K calculated from the following expression fitted well our entire conversion data:

$$K = \exp\left(\frac{1}{\phi - \phi_c}\right) \tag{6}$$

Thus, the pore parameters and the reaction rate can now be related as

$$\frac{d\phi}{dt} = \frac{M}{\rho} k_s C_{SO_2} a^A, \tag{7}$$

where M and ρ are the molecular weight and density of the reactant, and k_s and C_{SO_2} are the surface rate constant and the gas concentration at the specimen surface.

Artificial neural networks

ANN is a computational system based on pattern recognition achieved from intense learning of stored knowledge. ANN may be considered as a black box containing one or more computational logic units (CLU) connected in tandem. The first and last layers in this network are the input and output layers, respectively, with hidden layers present in between. While the input and target values are obtained from observation, the values in the hidden layers are found by training with the help of an external teacher that optimizes the values through error signals and bias corrections. When the training is complete, the converged net has the ability to recognize and generalize the patterns intrinsic to the training set.

ANNs are designed to simulate the brain's learning process, the fundamental unit of which, the nerve cell, is represented in ANN by computational units called neurons. In the human neural networks, the degree of response (the output) to a stimulus (an input) is believed to be a function of the strength of neural connections known as synaptic strength, represented in ANN by weights and biases. To train ANNs, then, the inputs are multiplied by *weights* of random values, and in a multilayered feedforward network weights are found that match the input with the target values using an error backpropagation algorithm (Rumelhurt et al., 1986). Specifically, if $I_{j,p}$ represent the inputs, then the weighted average inputs ($W_{i,j}I_{j,p}$) are summed up with a bias, u_i, Eq. 8. The result, ($Y_{i,p}$), is squashed by a nonlinear transformation to form the input of the subsequent layer, Eq. 9

$$Y_{i,p} = \sum_{j=1}^{n} W_{i,j} \times I_{j,p} + u_i \tag{8}$$

$$Z_{i,p} = \frac{1}{1+\exp(-Y_{i,p})}, \tag{9}$$

where j is the number of originating nodes (input node), i is the number of nodes in the next immediate layer, and p is the number of patterns. This process is repeated for all the layers of the network, as shown in Figure 2. If we denote the output of the kth neuron as $O_{k,p}$, the computed output from this neural layer is compared with the given target value. Then the error for a particular pattern, p, at the final layer is calculated as

$$E_p = (T_{k,p} - O_{k,p}), \tag{10}$$

where $T_{k,p}$ is the desired output. Finally, the objective function, obtained by summing up the error for one complete set of pattern ($E = \Sigma_p \Sigma_k E_{k,p}$), is minimized by adjusting the weights by the following relation (Rumelhart et al., 1986):

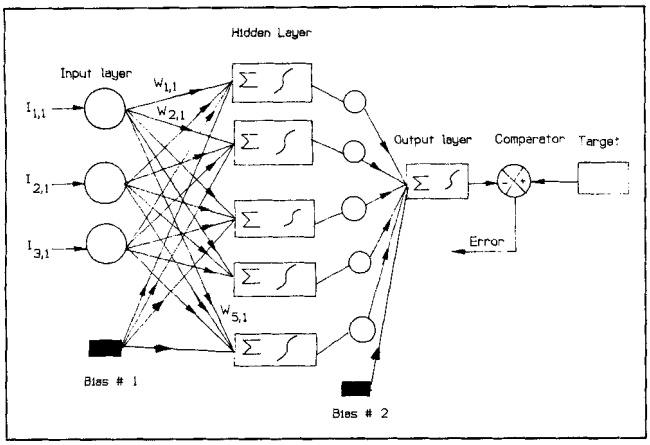

Figure 2. Artificial neural network applied in this study.

$$\Delta W_{i,j}^{n+1} = \eta\left(-\frac{\delta E}{\delta W_{i,j}}\right) + \alpha \Delta W_{i,j}^{n}, \qquad (11)$$

where η is the learning rate and α is the momentum correction factor that helps in damping the oscillations in the weight change. The calculation of local gradient ($\delta E/\delta W_{i,j}$) depends on whether the neuron is in the output layer or in the hidden layer. The ANN employed in this study is shown in Figure 2.

Results and Discussion

Limestone-SO_2 reaction

These limestone types, as other varieties of limestone, are mainly made of the mineral calcite. The mineralogical composition of these limestone as determined by an X-ray diffraction technique (see Methods section) is given in Table 1. The ionic composition of solution obtained by the digestion of these limestones in HCl showed that, in addition to the preponderant Ca^{2+}, Mg^{2+} was also present but was in all cases less than 1 wt. % of Ca^{2+}. Thus, the conversion of limestone in an SO_2 environment can be evaluated on the basis of $SO_2 - CaCO_3$ reaction only, as shown by the following equations.

$$CaCO_3 + SO_2 + \frac{1}{2}H_2O \rightarrow CaSO_3 \cdot \frac{1}{2}H_2O + CO_2 \qquad (12)$$

$$CaSO_3 \cdot \frac{1}{2}H_2O + \frac{1}{2}O_2 + 1\frac{1}{2}H_2O \rightarrow CaSO_4 \cdot 2H_2O. \qquad (13)$$

Table 1. Mineralogical Composition of the Limestone Varieties

Limestone Type	Calcite %	Quartz %
CR	99.7	0.3
CS	99.7	0.3
LD	97.0	3.0
BD	99.0	1.0

Note: Cordova Cream (CR), Cordova Shell (CS), Louder (LD), and Bedford (BD).

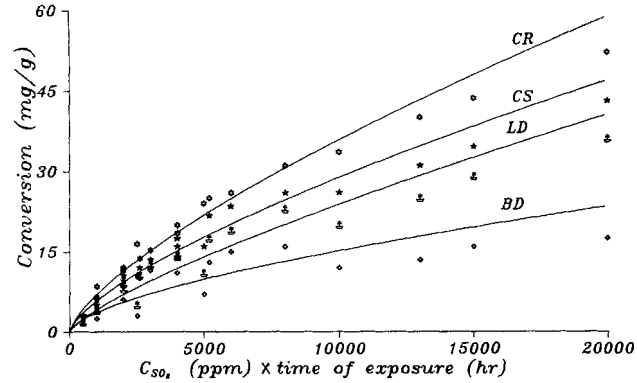

(a)

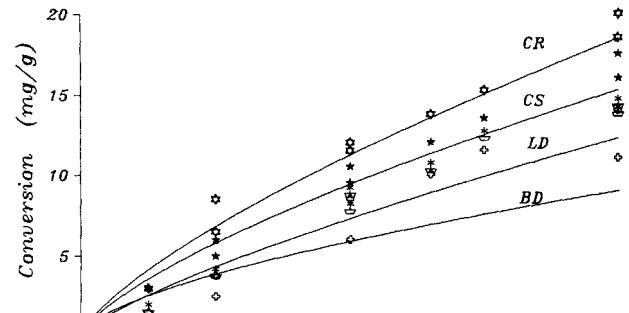

(b)

Figure 3. Reaction rate by regression of data of samples exposed to 10, 20 and 50 ppm of SO_2 for periods up to 400 h.

Symbols represent experimental values. CR, CS, LD, and BD are Cordova Cream, Cordova Shell, Louder, and Bedford limestone, respectively. (a) All available conversion data are shown. (b) Conversion data for values < 4000 ppm $\times$ h to show that a better correlation exists than shown in part (a) when the data span all SO_2 concentrations used.

The SO_2 reacts with the specimen at the surface, producing a crust of gypsum, $CaSO_4 \cdot 2H_2O$. The crust grows outward in continued reaction by the transport of Ca^{2+} from the unaltered limestone and the resulting reaction of Ca^{2+} with SO_2 at the sample surface (Skoulikidis and Charalambous, 1981; Gauri et al., 1992). The details of the formation of gypsum crust, its evolution, morphology, and composition are discussed in Gauri et al. (1989). Underneath the crust, in the unaltered limestone, cavities form by enlargement of the pore space resulting from the depletion of Ca^{2+}. The mass of gypsum formed and the resulting new porosity created are the measures of the conversion of the parent limestone. We present below results of experimental study on conversion vs. time for the various varieties of limestone.

Figure 3 is a composite profile comparing conversions of all limestone types exposed in 10, 20 and 50 ppm SO_2 atmospheres. CR shows the maximum conversion and BD the least, depending upon the porosities and pore-size distributions (Table 2). CR has the largest porosity as well as a large volume of small pores that promote reaction by offering a large surface area.

Table 2. Porosity and Density of the Limestone Varieties

Sample Name	Initial Porosity %	Final Porosity %	Density g/cm^3
CR	26.13	27.50	1.97
CS	21.65	22.67	2.08
LD	19.94	21.23	2.14
BD	13.74	14.56	2.29

Note: Cordova Cream (CR), Cordova Shell (CS), Louder (LD), and Bedford (BD). The final porosity was measured after the reaction product had been leached.

Figure 3a shows that the correlation of data in the lower than 5,000 ppm·h regime is excellent; this is shown more clearly in Figure 3b. Not so good a correlation in the higher than 5,000 ppm·h region is perhaps due to the few available points that represent reaction in a 50-ppm SO_2 atmosphere only, whereas the data points in the lower region represent reaction in all SO_2 concentrations used.

Figure 4a represents trajectories of the reaction rate curves for CR and CS, showing declining rates in prolonged exposure. This is particularly true when the rate curves for reaction in a 50-ppm SO_2 atmosphere is considered. These changes in the reaction rates can be attributed to the large mass of the reaction product formed, offering greater resistance to the diffusion of the reactant species. This explanation is supported by the linear trajectories of the rate curves in BD and LD (Figure 4b), which due to relatively low porosities experience overall lower conversions. In general, the reaction-rate curves may be considered to follow a linear or a quasi-linear path in all four varieties of the limestone.

The mechanism of reaction of limestone in an SO_2 atmosphere just described lends itself to evaluation by the shrinking unreacted core model and a percolation theory model. We will apply these commonly used models to evaluate these reactions as well as show that our first time application of ANN can also effectively evaluate these gas–solid reactions.

Evaluation of reaction based upon mathematical models

Application of Shrinking Unreacted Core Model. To fit this model, the kinetic constants, namely, the rate constant (k_s) and the order of the reaction (found to be a nearly first order) were obtained from time-conversion data by nonlinear regression analysis (DRNLIN of IMSL subroutine, 1989). The k_s values are, 1.51, 0.9, 0.16 and 0.09 (cm/h) for CR, CS, LD and BD, respectively. To match the time profile the solid-state effective diffusivity (D_e) values for CR, CS, LD, and BD were found to be $3.5\pm0.07\times10^{-12}$, $1.32\pm0.08\times10^{-12}$, $2.52\pm0.25\times10^{-11}$, and $4.79\pm0.9\times10^{-13}$ (cm^2/s), respectively. The results of integration (Eq. 2) of these data are plotted in Figures 5a–5d, showing that the shrinking unreacted core model fits the experimental data well.

Application of Distributed Pore Model. As seen from Eqs. 4–7, the elements needed to apply this model are the surface rate constant and pore-structure properties such as porosity, a pore coordination number, and the related K factor. Initial sedimentation processes created a microporosity that was modified by circulating waters as these limestones were lifted above the sea level, creating some large pores. Further, many shells of organisms, which were incorporated in the rock possess intricate porosities of their own. Thus, due to many unconnected pore structures found in these rocks we have modeled the system in the Bethe lattice concept in order to determine various percolation properties analytically.

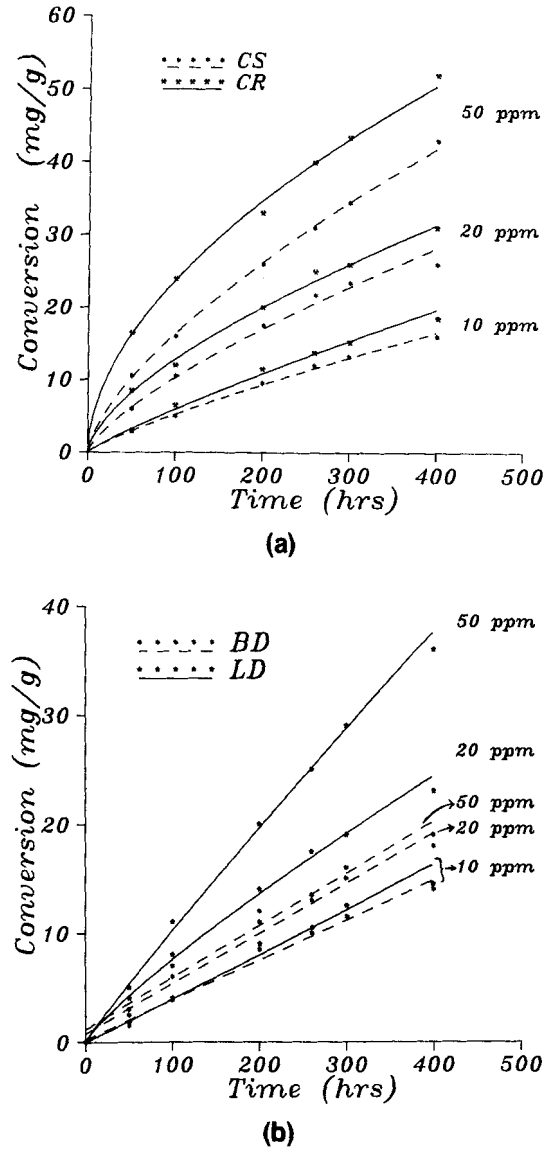

Figure 4. Conversion time of the limestone varieties studied.

The curves are drawn on the basis of regression analysis; symbols represent experimental values. (a) Cordova Cream and Cordova Shell. (b) Louder and Bedford.

The initial porosity, the end porosity, and the bulk density of the limestone varieties studied are shown in Table 2. While the rate constant, k_s, was determined from the regression analysis of the experimental data (shown in the preceding section on shrinking core model), K was evaluated using total and critical porosity (Eq. 6) and not by matching initial surface area measurement (Reyes and Jensen, 1986). The conversion-time plot for various limestones is shown in Figures 5a–5d, using model Eqs. 4–7. The Z value ranged from 10 to 14. This value is higher than that conventionally used in percolation models, but seems to be real considering the complex network of pores. Further, this value gives the best fit to observed conversions of all varieties of limestone.

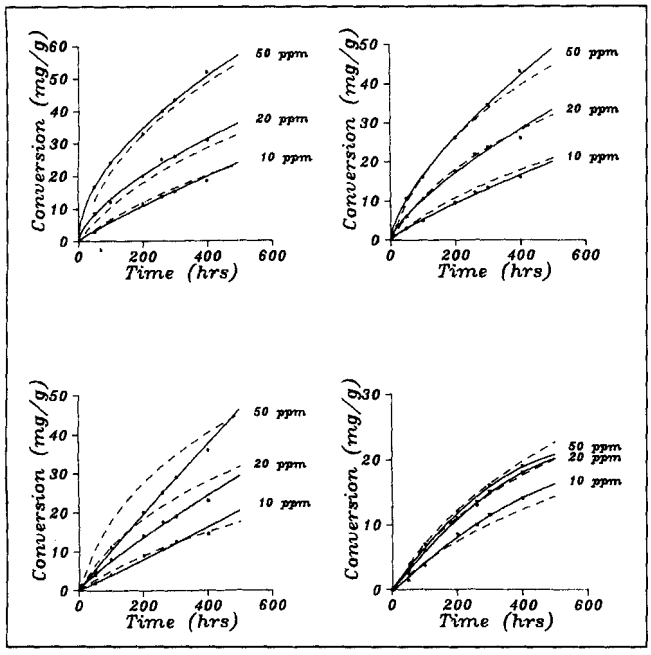

Figure 5. Conversion time predicted by the shrinking unreacted core model (solid line) and the distributed pore model (dotted line).

(a) Cordova Cream; (b) Cordova Shell; (c) Louder; and (d) Bedford. Symbols denote experimental values.

Percolation theory has been applied for modeling gas–solid reactions where a large change in porosity, 20% or more, had occurred (Reyes and Jensen, 1986). In our experiments the porosity changed by only 1.4%, at best showing that the pore model is applicable to situations where the maximum conversion due to reaction is rather low.

Application of ANN. The application of ANN to gas–solid reactions is the major concern of this article. Therefore, we will describe the procedure used in greater detail than we have done in the case of other models. We will also discuss why we believe that ANN is superior for predicting gas–solid reactions than multivariate regression techniques that may also be applied for the purpose.

The network architecture we have used has an input layer with three neurons, one hidden layer with five neurons, an output layer with one neuron, and a target value. Porosity, density, and a selected data point representing a ppm×h of reaction for a specimen are the elements of the input layer designated as $I_{1,p}$, $I_{2,p}$, and $I_{3,p}$ in Figure 2. As a first step in the operation of ANN these input values are multiplied by randomly selected weights ($W_{i,j}$, $i=1,\ldots,5$; $j=1,\ldots,3$) and summed up and processed in the hidden layer according to Eq. 9. This step is then repeated to yield data for the subsequent layer, which in our architecture is the output layer. The value in the output layer is then compared with the target, which is the observed conversion for a given period of reaction. This input-target pair forms a pattern. For the selected three limestone varieties (CR, LD, and BD) and three periods of conversion (500, 1,000 and 2,000 ppm×h) patterns were obtained. Using the backpropagation algorithm (Rummelhart et al., 1986), the network was then trained to minimize the error, that is, the difference of values between the output layer and the target. The weights were updated as needed so that the error was minimized. This process was repeated until the error reached a significantly low predefined value.

The learning coefficient, η, and the momentum correction factor, α, for the entire training phase were kept to a constant at 0.3 and 0.05, respectively. A complete sweep of input-target data for each pattern following Eq. 11 resulted in the training of ANN.

Figure 6 shows the plots of experimental points as well as the curves predicted by the application of converged weights determined. A good correlation exists between the experimental and the predicted values, even for longer periods of reaction than experimental data that had not been included in the training phase. In addition, the conversion of the CS limestone that also was not used for training was correctly predicted.

Further, we used the weights obtained earlier to predict conversion of BD limestone used in the construction of tombstones exposed in Cave Hill cemetery in Louisville, where a nearly 20 ppb SO_2 concentration was found to exist during the period of exposure. We calculated that a nearly 3-μm-thick crust would form in one year. This result compares well with the nearly 2-μm crust thickness formed upon marble in a year in the Louisville area (Yerrapragada et al., 1994).

While it is known that porosity characteristics influence the progress of reaction, many porosity-related properties cannot be determined by known techniques, and thus cannot be used in any modeling effort. Pore geometry and pore connectivity, for instance, cannot be quantified, yet these are two features that conceptually are highly significant in driving the reaction. Even though these properties cannot be determined by

Table 3. Mercury Intrusion Porosimetry of the Limestone Varieties

Sample Name	Large Pores (LP) > 50 μm	Necks (N) 10–50 μm	Small Pores (SP) < 10μm	(LP+N) /SP
CR	0.0536	0.0024	0.0830	0.64
CS	0.0570	0.0210	0.0580	0.98
LD	0.0520	0.0040	0.0370	1.40
BD	0.0300	0.0050	0.0420	0.71

Note: Cordova Cream (CR), Cordova Shell (CS), Louder (LD), and Bedford (BD). The pore size is in μm diameter, and the pore volume, shown for each category of pores, is in cc/g.

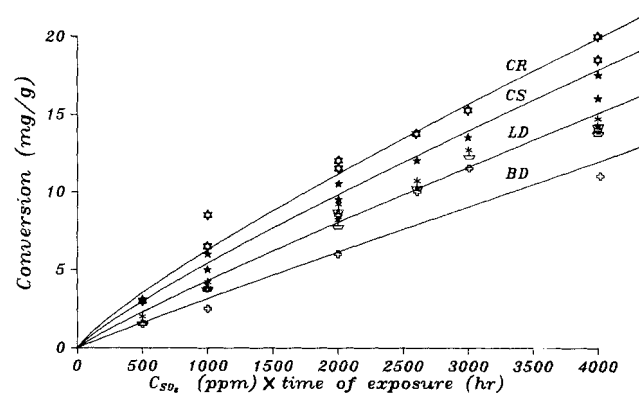

Figure 6. Reaction rate predicted by ANN.

Symbols denote experimental values.

the use of ANN, ANN has been proved suitable to predict the magnitude of conversions because its main power is in pattern recognition.

Further, ANN, seemingly a regression technique, differs from and is superior to routinely applied regression techniques. For instance, in ANN no single node is responsible for associating a certain input with an output. Instead, each node encodes a microfeature of the input–output pattern. When we assemble all the nodes together into an ordered coordinated network by adjusting the strength of the connecting nodes with the help of training algorithms, these microfeatures encode the macroscopic input–output pattern. If process conditions change, ANN can be subjected to further training and updated to match the input–output performance, making it a self-correcting model. Finally, most regression techniques map one, two, or at the most three dependent variables, whereas ANN can map many dependent and independent variables.

The ability of ANN to recognize patterns has been successfully utilized in evaluation of many diverse areas. To name just a few, ANN recognized hidden patterns in DNA (Hirst and Sternberg, 1992), in protein structure (Bohr et al., 1990), and in sequences that primarily regulate gene expressions (Nair et al., 1994). ANN has been applied in the solution of several problems in chemical engineering practice including fault diagnosis (Hoskins and Himmelblau, 1988), process control (Psaltis et al., 1988; Nguyen and Widrow, 1990), dynamic modeling (Bhat and Mcavoy, 1990), and forecasting in short noisy time series (Foster et al., 1990). Further, ANN has performed well in market forecasting (Chitra, 1993) and even in the classification of galaxies (Lahav et al., 1995), and in chaotic time-series prediction generated by an NH_3 laser (Wan, 1994), all of which require highly complex, nonlinear analysis. It is therefore not surprising that we have been able to train ANN to correctly predict the evolution of gas–solid reactions, which shows quasi-linear behavior.

Conclusion

We have trained artificial neural networks (ANNs) on the basis of certain physical properties of limestones and their conversion in SO_2-enriched atmospheres. The weights thus obtained have successfully predicted conversion of another limestone that was not used in the training phase. These weights have also correctly predicted the thickness of a crust formed upon marble in an ambient industrial atmospheres that has a much lower SO_2 concentration than those used for our experiments.

Acknowledgment

This research project on porous building stones is funded by the NSF under Grant BCS 9301059. We thank Dr. Sebastian Reyes for valuable discussions and Prof. John Sinai for helping in editing the manuscript. The Indiana and the Texas samples of limestone used in this study were furnished by the Indiana Limestone Co., Bedford and Texas Quarries, Cedar Park, respectively. We thank all these for their support.

Literature Cited

Bhat, N., and T. J. Mcavoy, "Use of Neural Nets for Dynamic Modeling and Control of Chemical Process Systems," *Comput. Chem. Eng.*, **14**(4/5), 573 (1990).

Bhatia, S. K., and D. D. Perlmutter, "A Random Pore Model for Fluid-Solid Reactions: I. Isothermal, Kinetic Control," *AIChE J.*, **26**(3), 379 (1980).

Bohr, H., J. Bohr, S. Brunak, R. M. J. Cotterill, B. Lautrup, L. Norskov, O. H. Olsen, and S. B. Peterson, "A Novel Approach to Prediction of the 3-Dimensional Structures of Protein Backbones by Neural Networks," *FEBS Lett.*, **261,** 43 (1990).

Cao, G., W. Strieder, and A. Varma, "Analysis and Shape Inequalities for Gas-Solid Reactions with Changing Volume," *AIChE J.* **41**(2), 324 (1995).

Chitra, S. P., "Use Neural Networks for Problem Solving," *Chem. Eng. Prog.*, 44 (Apr., 1993).

Chowdhury, A. N., A. R. Punuru, and K. L. Gauri, "Weathering of Limestone Beds at the Great Sphinx," *Environ. Geol. Water Sci.*, **15**(3), 217 (1990).

Doraiswamy, L. K., and M. M. Sharma, *Heterogeneous Reactions: Analysis, Examples, and Reactor Design*, Wiley, New York (1984).

Fisher, M. E., and J. W. Essam, "Some Cluster Size and Percolation Problems," *J. Math. Phys.*, **2**, 609 (1961).

Foster, W., F. Collopy, and L. Ungar, "Neural Network for Forecasting Short Noisy Time Series," AIChE Meeting, Chicago (1990).

Fuertes, A. B., and G. Marban, "Modelling of Gasification Reaction Including the Percolation Phenomenon," *Chem. Eng. Sci.*, **49**(22), 3813 (1994).

Gauri, K. L., N. P. Kulshreshtha, A. R. Punuru, and A. N. Chowdhury, "Rate of Decay of Marble in Laboratory and Outdoor Exposure," *J. Mater. Civil Eng.*, **1**, 73 (1989).

Gauri, K. L., S. S. Tambe, and E. N. Caner-saltik, "Weathering of Dolomite in Industrial Environments," *Environ. Geol. Water Sci.*, **19**(1), 55 (1992).

Hartman, M., and R. W. Coughlin, "Reaction of Sulfur Dioxide with Limestone and the Grain Model," *AIChE J.*, **22**(3), 490 (1976).

Hirst, J. D., and J. E. M. Sternberg, "Prediction of Structural and Functional Features of Protein and Nucleic Acid Sequences by Artificial Neural Networks," *Biochemistry*, **31,** 7211 (1992).

Hoskins, J. C., and D. M. Himmelblau, "Artificial Neural Network Models of Knowledge Representation in Chemical Engineering," *Comput. Chem. Eng.*, **12**(9/10), 881 (1988).

IMSL Math/Library, FORTRAN subroutines for Mathematical Applications (1989).

Lahav, O., A. Nain, R. J. Buta, H. G. Corwin, A. Dressler, Vaucoulers, J. P. Huchra, S. van den Bergh, S. Raychaudhury, L. Sodfe, Jr., and M. C. Storrie-Lombardi, "Galaxies, Human Eyes and Artificial Neural Networks," *Science*, **267,** 859 (1995).

Mohanty, K. K., J. M. Ottino, and H. T. Davis, "Reaction and Transport in Disordered Composite Media: Introduction of Percolation Concepts," *Chem. Eng. Sci.*, **37,** 905 (1994).

Nair, T. M., S. S. Tambe, and B. D. Kulkarni, "Application of Artificial Neural Networks for Prokaryotic Transcription Terminator Prediction," *FEBS Lett.*, **346,** 273 (1994).

Nguyen, D. H., and B. Widrow, "Neural Networks for Self-Learning Control Systems," *IEEE Contr. Sys. Mag.*, 18 (Apr., 1990).

Psaltis, D., A. Sideris, and A. A. Yamamura, "A Multilayered Neural Network Controller," *IEEE Contr. Syst. Mag.*, 17 (Apr., 1988).

Reyes, S., and K. F. Jensen, "Percolation Concepts in Modelling of Gas-Solid Reactions: I. Application to Char Gasification in the Kinetic Regime," *Chem. Eng. Sci.*, **41**(2), 333 (1986).

Rumelhart, D., G. Hilton, and R. Williams, "Learning Representations by Backpropagating Errors," *Nature*, **323,** 533 (1986).

Skoulikidis, Th., and D. Charalambous, "Mechanism of Sulphation by Atmospheric SO_2 of the Limestone and Marbles of Ancient Monuments and Statues," *Br. Corro. J.*, **16,** 70 (1981).

Snow, M. J. H., J. P. Longwell, and A. F. Sarofim, "Direct Sulfation of Calcium Carbonate," *Ind. Eng. Chem. Res.*, **27,** 268 (1988).

Szekely, J. J., J. W. Evans, and H. Y. Sohn, *Gas-Solid Reactions*, Academic Press, New York (1976).

Tambe, S., K. L. Gauri, S. Li, and W. G. Cobourn, "Kinetic Study of SO_2 Reaction with Dolomite," *Environ. Sci. Technol.*, **25**(12), 2071 (1991).

Tambe, S., S. S. Yerrapragada, and K. L. Gauri, "Kinetics of SO_2-Dolomite Reaction: Application of Random Pore Model," *J. Mat. Civil Eng.*, **6**(1), 65 (1994).

Wan, E. A., "Time Series Prediction by Using a Connectionist Network with Internal Delay Lines," *Time Series Prediction: Forecasting*

the Future and Understanding the Past, A. S. Weigend and N. A. Gershenfeld, eds., Addison-Wesley Co., Reading, MA, p. 195 (1994).
Washburn, E. W., "Note on a Method of Determining the Distribution of Pore Size in a Porous Material," *Proc. Natl. Acad. Sci.*, U.S.A., 7, 115 (1921).
Weast, R. C., ed., *CRC Handbook of Chemistry and Physics*, CRC Press, Boca Raton, FL (1974).
Yerrapragada, S. S., J. H. Jaynes, S. R. Chirra, and K. L. Gauri, "Rate of Weathering of Marble Due to Dry Deposition of Ambient Sulfur and Nitrogen Dioxides," *Anal. Chem.*, **66**(5), 655 (1994).
Yerrapragada, S. S., S. S. Tambe, and K. L. Gauri, "Fractals, Pore Potential, and Sphinx Limestone Durability," *Rocks for Erosion Control, ASTM STP 1177*, C. H. McElroy and D. A. Lienhart, eds., p. 38 (1992).
Yortsos, Y. C., and M. Sharma, "Application of Percolation Theory to Noncatalytic Gas-Solid Reactions," *AIChE J.*, **32**(1), 46 (1986).
Zarkanitis, S., and S. V. Sotirchos, "Pore Structure and Particle Size Effects on Limestone Capacity for SO_2 Removal," *AIChE J.*, **35**(5), 821 (1989).

Manuscript received May 22, 1995, and revision received Dec. 15, 1995.